Medical Engineering and Physics 37 (2015) 759–766

Contents lists available at ScienceDirect

Medical Engineering and Physics

journal homepage: www.elsevier.com/locate/medengphy

Biomechanical properties of the Marfan's aortic root and ascending aorta before and after personalised external aortic root support surgery

S.D. Singh [a], X.Y. Xu [a,*], J.R. Pepper [b,c], T. Treasure [d], R.H. Mohiaddin [b,c]

[a] Department of Chemical Engineering, Imperial College London, South Kensington Campus, London SW7 2AZ, UK
[b] Royal Brompton and Harefield NHS Foundation Trust, Sydney Street, London SW3 6NP, UK
[c] National Heart and Lung Institute, Imperial College London, London SW7 2AZ, UK
[d] Clinical Operational Research, Department of Mathematics, University College London, 4 Taviton Street, London WC1H 0BT, UK

ARTICLE INFO

Article history:
Received 11 August 2014
Revised 16 February 2015
Accepted 9 May 2015

Keywords:
Marfan syndrome
Aortic root dilatation
Finite element modelling
Vascular prosthetics

ABSTRACT

Marfan syndrome is an inherited systemic connective tissue disease which may lead to aortic root disease causing dilatation, dissection and rupture of the aorta. The standard treatment is a major operation involving either an artificial valve and aorta or a complex valve repair. More recently, a personalised external aortic root support (PEARS) has been used to strengthen the aorta at an earlier stage of the disease avoiding risk of both rupture and major surgery. The aim of this study was to compare the stress and strain fields of the Marfan aortic root and ascending aorta before and after insertion of PEARS in order to understand its biomechanical implications.

Finite element (FE) models were developed using patient-specific aortic geometries reconstructed from pre and post-PEARS magnetic resonance images in three Marfan patients. For the post-PEARS model, two scenarios were investigated—a bilayer model where PEARS and the aortic wall were treated as separate layers, and a single-layer model where PEARS was incorporated into the aortic wall. The wall and PEARS materials were assumed to be isotropic, incompressible and linearly elastic. A static load on the inner wall corresponding to the patients' pulse pressure was applied.

Results from our FE models with patient-specific geometries show that peak aortic stresses and displacements before PEARS were located at the sinuses of Valsalva but following PEARS surgery, these peak values were shifted to the aortic arch, particularly at the interface between the supported and unsupported aorta. Further studies are required to assess the statistical significance of these findings and how PEARS compares with the standard treatment.

1. Introduction

Marfan syndrome (MFS) is a heritable systemic connective tissue disorder with manifestations in the cardiovascular, ocular and skeletal systems [1]. Cardiovascular complications of MFS are the major cause of death in patients with this disease [2]. MFS is linked to mutations in the fibrillin 1 gene (FBN1), which is responsible for the synthesis of normal fibrillin glycoprotein. This protein is a major component of microfibrils [3]. In MFS, the structural microfibril abnormalities not only result in inherently weakened aortic connective tissue, but also in failure of the normal maintenance and repair processes. The interplay of aortic biomechanics and the abnormal aortic wall connective tissue is conducive for the formation of aortic aneurysm [4]. Normally, elastic fibres enable the aorta to distend during the cyclic increase of blood pressure and then recover fully to its original state upon removal of the pressure load. However, fragmentation of the elastic fibres prevents full recovery from the cyclic distending pressure. This results in a thinned aortic wall which exhibits progressive aortic dilatation and decreased distensibility with heightened risks of aneurysm formation and dissection throughout the length, but mainly at the root [5,6]. Dilated aortic root in MFS is typically characterised by increases in diameter across the sinuses of Valsalva and the sinotubular junction with cranial displacement of the origin of the coronary arteries and often incompetent aortic valve [6]. Currently, for patients with MFS exhibiting dilating aortic root and ascending aorta, the threshold for intervention has fallen between 45 and 50 mm diameter, especially if progressive dilatation is observed [6].

Various surgical techniques have been used to repair the dilated aortic root, aorta and the leaking aortic valve in MFS. The standard surgical approach (known as the Bentall procedure) is the composite root replacement in which a mechanical prosthetic valve is sewn into

* Corresponding author: Tel.: +44 207 594 5588; fax: +44 207 594 1989.
E-mail address: yun.xu@imperial.ac.uk (X.Y. Xu).

http://dx.doi.org/10.1016/j.medengphy.2015.05.010
1350-4533/

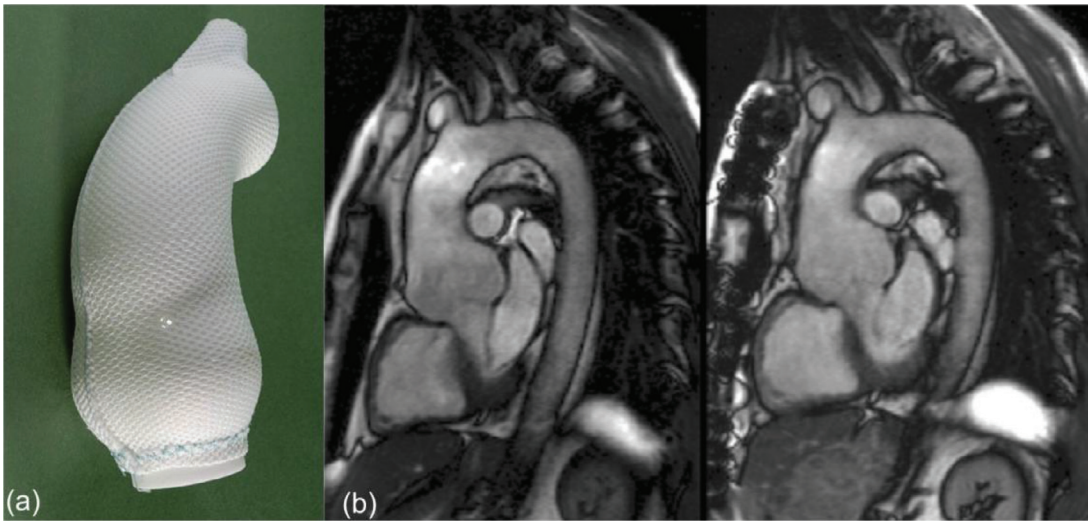

Fig. 1. (a) Aortic model wrapped in the personalised external aortic root support (PEARS) which is manufactured from a medical grade mesh; (b) Magnetic resonance imaging of the aorta before (left) and after (right) insertion of the PEARS in the first patient [11].

the proximal end of a Dacron tube graft [7]. The diseased aortic root and ascending aorta are replaced by a tube graft and the coronary ostia anastomosed to the side of the graft. Another option is the valve sparing root replacement which involves radical excision of the aortic root down to, but not including, the valve leaflets [8]. This is a more difficult operation requiring considerable operative skill and judgement [5,9]. More recently, a less invasive surgical technique has been pioneered and evaluated [10]. A personalised external aortic root support (PEARS) (shown in Fig. 1) is used to reinforce the ascending aorta while leaving the native aortic valve intact.

Early clinical results of PEARS indicated that there is no further dilatation of the aortic root after insertion of the PEARS, although the long term outcome cannot be predicted based on such early and limited experience [11,12]. Additionally, the structural status of the aortic wall after PEARS is uncertain [13]. To address these uncertainties, a macroscopic and histological evaluation was performed by wrapping polytetrafluoroethylene (PTFE) mesh, as used for the PEARS, around the carotid artery of sheep [14]. It was shown that the mesh became incorporated in the periadventitial tissue of the artery and there was a significant increase in the tensile strength of the carotid artery/mesh composite compared with the unwrapped carotid artery. One of the concerns associated with implantation of the PEARS is that the increasing stiffness of the supported aorta will affect the working load of the heart, mechanics of the valve and arterial pressures [14]. Additionally, the aorta distal to the support is unprotected and can be vulnerable to dilatation, a limitation shared by the Bentall procedure [12].

The combination of cardiovascular magnetic resonance imaging and finite element (FE) analysis offer the opportunity for detailed assessment of the biomechanical changes of the aortic root and ascending aorta before and after insertion of PEARS. Previous FE studies of the dilated aortic root include work done by Auricchio et al. [15] to reproduce aortic root pathology for assessment of aortic valve incompetence [15,16] to determine the mechanisms of aortic valve incompetence by applying radial forces to the root. However, none of these studies employed patient-specific geometries. One of the most important components of FE analysis is the selection of an appropriate constitutive model and the corresponding material properties. So far, several *in vivo* studies have reported the distensibility of the Marfan aorta [17–21] but these data do not give any information about the strength of the tissue. Okamoto et al. [22] determined the mechanical properties of dilated ascending aorta, particularly in patients with Marfan syndrome and bicuspid aortic valves, and applied these to a simplified model of the aorta [23]. The present study is not only the first attempt to evaluate the effects of the PEARS on the biomechanics of the Marfan aorta using patient-specific data, but also the first attempt at evaluating the biomechanics of the native Marfan aorta. Data from three patients were acquired before and after implantation of the PEARS and detailed analysis of stress patterns and displacements were carried out.

2. Methodology

2.1. MR image acquisition

Electrocardiographic-gated MR images of three Marfan patients, before and after implantation of the PEARS, were acquired from using a 1.5 Tesla scanner (Avanto, Siemens, Erlangen, Germany). Anatomical images used for segmentation of the aortic root and thoracic aorta were acquired in diastole, at the same point in the cardiac cycle. The images covered the ascending aorta, aortic arch and proximal descending aorta in three orthogonal planes (see Table 1 for imaging parameters) and were stored in a Digital Imaging and Communications in Medicine Data (DICOM) format. The study was approved by the local ethics committee, and complied with the Declaration of Helsinki.

2.2. Reconstruction of patient-specific ascending aorta

These DICOM images were imported into Mimics® (Materialise, Louvain, Belgium) segmentation software where a semi-automatic procedure was used for reconstruction. Two-dimensional (2D) region-growing method was used to detect the aortic lumen by defining seed-points in the region of interest and the lower and upper grey-level thresholds. The patient-specific 3D aortic lumen was then reconstructed by stacking 2D contours. The resulting geometry was smoothed to remove any noise from the surface, which might have resulted in artificial stress concentrations.

Two models describing the post-PEARS geometry were constructed, as illustrated in Fig. 2:

(i) A bilayer model, which was developed to simulate conditions immediately after insertion of the PEARS. It was assumed that the PEARS lay on the outer surface of the aortic wall upon its implantation. This was recreated by adding another layer corresponding to the thickness of PEARS from the aortic root to the base of the brachiocephalic artery of the pre-PEARS geometries.

Table 1
MR scan parameters of images used for reconstruction.

		Repetition time (ms)	Echo time (ms)	Flip angle (°)	Pixel size (mm)	Slice thickness (mm)	Interslice distance (mm)	Image frequency (MHz)
Patient 1	Pre	292.10	1.22	80	1.328	6.0	3	63.67
	Post	296.38	1.07	70	0.594	1.5	var.	63.67
Patient 2	Pre	221.00	1.40	90	0.781	0.8	0.8	63.68
	Post	251.00	1.45	70	0.625	2.0	2.0	63.68
Patient 3	Pre	338.87	1.22	80	1.328	6.0	3.0	63.68
	Post	292.10	1.22	80	1.328	6.0	3.0	63.68

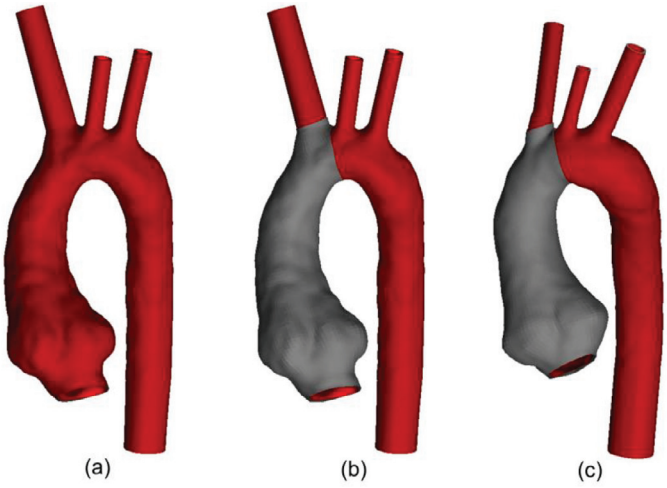

Fig. 2. Reconstructed patient-specific aortic geometries (a) pre-PEARS (b) post-PEARS, immediately after implantation of the PEARS (bi-layer model) and (c) post-PEARS, when the PEARS has become integrated into the periadventitial tissue.

(ii) A single-layer model, which was developed to simulate later stages when the PEARS became integrated into the aortic wall. The post-PEARS MR images were acquired between 1 and 4 years after implantation. From these images it was very difficult to identify a clear boundary between the aortic wall and the PEARS since the PEARS had become integrated with the outer layers of the wall. Hence, the integrated wall region was treated as a composite "wall-PEARS".

2.3. FE modelling strategy

ANSYS® ICEM CFD™ was used to discretise the resulting geometries using hexahedral elements. Mesh independence tests were performed using mesh sizes of 200,000, 300,000 and 400,000 elements. The differences in terms of peak displacement, peak stress and strain between the 200,000 element mesh and the 300,000 element mesh were less than 1.5% and those between the 300,000 and 400,000 element mesh were less than 1.0%. Consequently, mesh sizes greater than 300,000 were used in this study.

A linear elastic constitutive equation was adopted to describe the aortic wall, assuming it to be incompressible, homogenous and isotropic. The elastic moduli of the aortic wall and PEARS were obtained from previously reported experimental data [24,25]. Based on the sheep study by Verbrugghe et al. [14], the composite "wall-PEARS" showed approximately 125% increase in stiffness compared with the non-wrapped artery. These properties are summarised in Table 2, along with the Poisson's ratio and thickness of the wall. A uniform wall thickness was assigned owing to limitations in imaging resolution. These were based on previously reported data for Marfan wall [24] and PEARS [25]. However, for the Marfan wall-PEARS composite material, a total thickness of 1.5 mm was used to account for formation of a periarterial fibrotic sheet [14].

Table 2
Material properties used in the finite element models.

	Marfan wall	PEARS	Composite
Elastic modulus (kPa)	3000	7800	6750
Poisson's ratio	0.49	0.35	0.45
Wall thickness (mm)	1.0	0.3	1.5
References	[24]	[25]	[14]

Table 3
Patient data used in this study.

	Patient 1		Patient 2		Patient 3	
	Pre	Post	Pre	Post	Pre	Post
Blood pressure (mmHg)						
Systolic	135	130	110	110	118	110
Diastolic	78	70	60	60	84	70
Pulse	57	60	50	50	34	40
Aortic root diameter (mm)	37.0	38.7	39.4	39.7	39.3	39.2
Ascending aorta (mm)	22.7	22.9	29.3	27.0	29.0	27.0

The boundary conditions were then applied. These included nodal surface loads and displacement constraints. A static load corresponding to the patients' pulse pressure (Table 3) was applied perpendicular to the inner surface of the aorta. Zero-displacement constraints were set at the proximal aortic root, at the distal ends of the brachiocephalic, common carotid and left carotid arteries, and in the mid-descending aorta. The ANSYS structural solver (Ansys Inc., USA) was employed to obtain numerical solutions. Simulations were performed using a 16.0 GB RAM personal computer with Intel® Core™ i7-2600 3.40 GHz, running Windows 7 Enterprise.

3. Results

3.1. Anatomical features

Fig. 3 illustrates the inner surfaces of the pre-PEARS and post-PEARS aortas reconstructed from the corresponding MR images. Since the aortic branches were not often well-defined in these images, they were extended artificially to reduce the end effects. The descending aorta was also extended artificially for this reason. Additionally, the pre-PEARS images of Patient 2 resulted in four branches being reconstructed from the aortic arch. However, this extra branch was not captured clearly in the post-PEARS images of the same patient therefore it was removed from the pre-PEARS images for comparative purposes. Key geometric parameters corresponding to the pre- and post-PEARS geometries are given in Table 3, along with measurements of blood pressure.

3.2. Displacement

Upon addition of the external support and further integration into the aortic wall, the total displacement of the aortic wall was significantly reduced, particularly in the aortic root and sinuses of Valsalva. Fig. 4 shows the maximum total displacement in the sinuses, and its

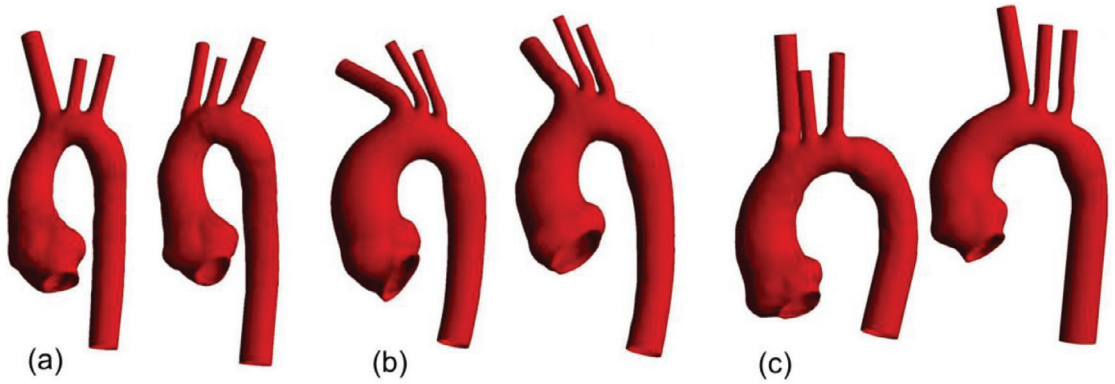

Fig. 3. Pre-PEARS (left) and post-PEARS (right) luminal surfaces reconstructed from patient-specific magnetic resonance imaging (MRI) for (a) Patient 1, (b) Patient 2 and (c) Patient 3, respectively.

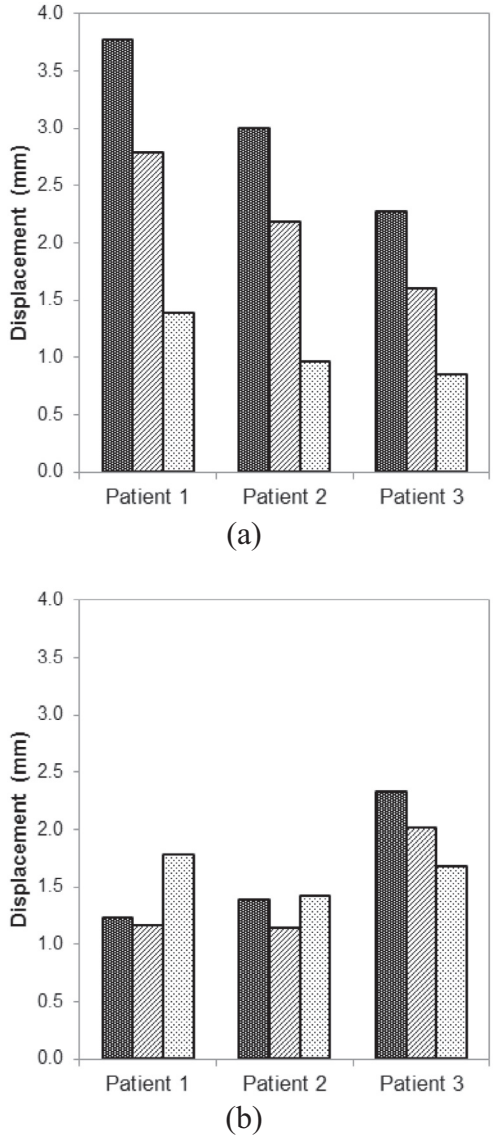

Fig. 4. Maximum total displacement in the sinus of Valsalva (a) and aortic arch (b) obtained from the ▦ Pre-PEARS, ▨ Post-PEARS (bilayer) and ⚃ Post-PEARS (single-layer) models for Patients 1, 2 and 3.

comparison with the displacement in the aortic arch, for each patient in every model. The post-PEARS bilayer model is seen to have reduced displacements, both in the sinuses and the aortic arch, when compared to the pre-PEARS models. Cross-sectional views of total displacements in the sinuses of Valsalva are presented in Fig. 5, which clearly illustrates the reduction in displacement upon addition of the PEARS via the bilayer and single-layer models. In the pre-PEARS and post-PEARS bilayer models, the maximum displacements were located between the sinuses of Valsalva for Patients 1 and 2. In Patient 3, however, the maximum displacement was found on the aortic arch. In contrast, the maximum displacements obtained from the post-PEARS single-layer models were all located distal to the aortic arch, that is, the location of the maximum displacement shifted from the sinuses to unsupported regions in and around the aortic arch.

3.3. Stress distribution

In the pre-PEARS geometries, the ascending aorta and aortic arch generally had higher von Mises stresses than regions distal to the aortic arch, with the peak stresses located between the sinuses of Valsalva, as seen in Fig. 6. In the post-PEARS bilayer models, which simulate the biomechanical conditions immediately after insertion of the PEARS, similar patterns were observed with the peak stresses also being located between the sinus for Patients 1 and 2, but at the interface between the supported and unsupported region for Patient 3.

The magnitude of the peak stress was significantly larger in the post-PEARS bilayer model for Patients 1 and 2 but almost the same in Patient 3, as illustrated in Fig. 7. In contrast, the single-layer model had significantly reduced stresses in the sinus of all models while the peak stresses were located at the interface between the supported and unsupported aorta. Fig. 8 illustrates regions of stress greater than 290 kPa in the post-PEARS single-layer models for all three patients. Previous studies showed that peak stresses of an aneurysmal aorta were between 290 and 450 kPa [26]. As a conservative comparison to a known reference value, 290 kPa was chosen to highlight the high stress regions.

4. Discussion

Upon reconstruction, small differences in the shape and orientation of the aorta were observed. In the post-PEARS images, discrimination of the aortic wall from the PEARS was difficult, if not impossible, due to integration of the PEARS into the wall. The main purpose of the PEARS is to provide an additional support for an otherwise weakened structure prone to progressive dilatation and eventually dissection. In this manner, the PEARS allows the aorta to expand and recoil without the risk of dilatation. The PTFE mesh used to manufacture the PEARS is approximately 2.6 times stiffer than the

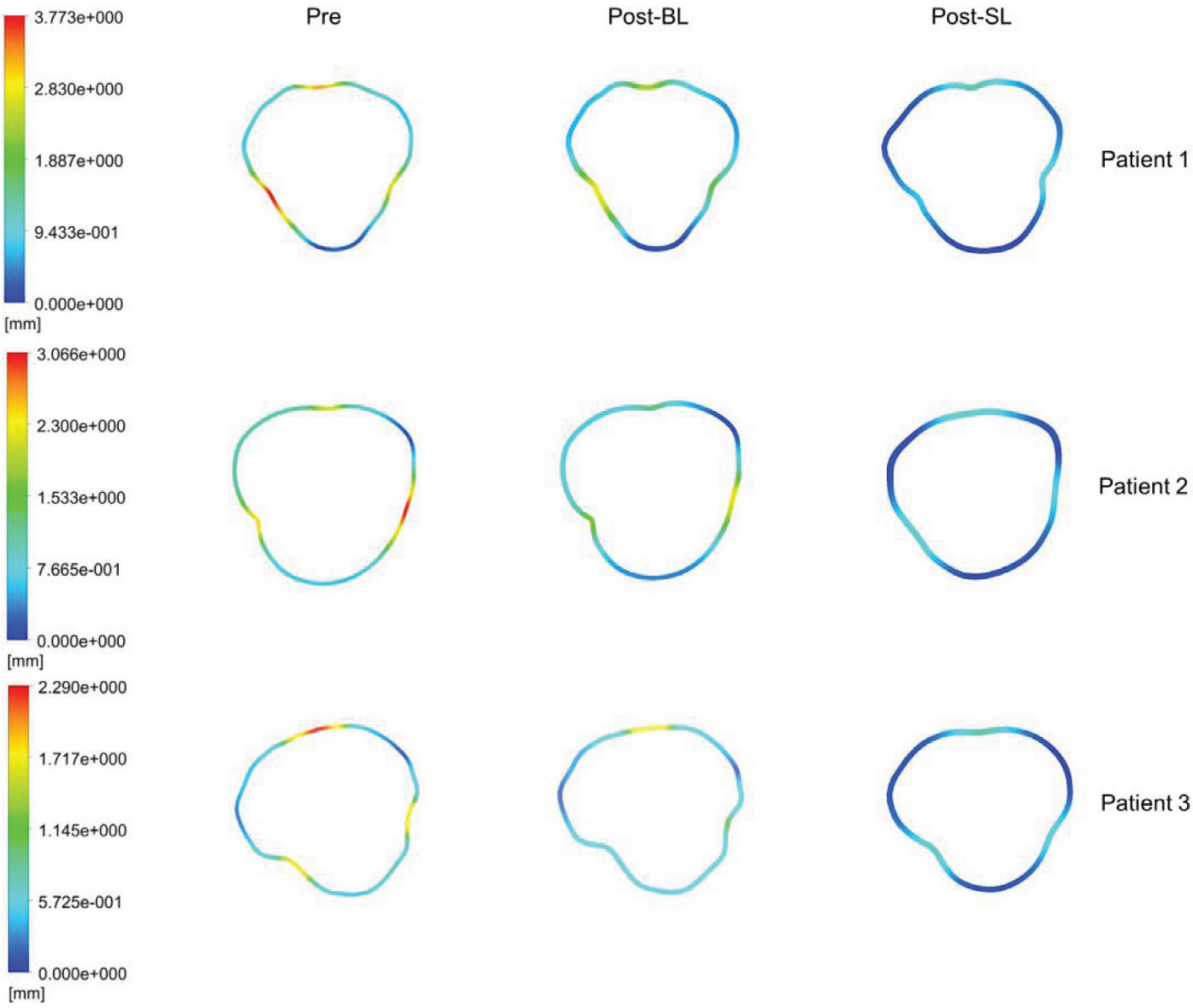

Fig. 5. Cross-sectional view of total displacements at the sinus of Valsalva pre-PEARS (left) and post-PEARS (middle: bilayer model; right: single-layer model).

Marfan aortic wall [24,25]. The material itself is less stiff than the material generally used (Hemashield, Dacron) to perform the Bentall or valve-sparing root replacements. The mesh used in the PEARS procedure is designed so that the hoop strength of the sleeve is greatest at the aorto-ventricular junction and gradually diminishes towards the aortic arch.

Based on the results obtained, the integration of the PEARS (post-PEARS single-layer model) showed reductions in the wall displacement of 63%, 68% and 62% in Patients 1, 2 and 3 respectively, in regions in and around the sinuses of Valsalva. These regions are known to exhibit progressive aortic dilatation and hence, maintaining the aortic diameters stable in the sinuses is important. However, reduction of the displacement in these areas also corresponded to the maximum displacement being shifted distally to the aortic arch, near the intersection between the supported and unsupported aorta. The magnitude of the maximum displacement was nevertheless significantly smaller than the maximum value observed before implantation of the PEARS (in the sinus). However, a local analysis showed that the aortic arch was now subjected to increased displacements of 44% and 3% in Patients 1 and 2 and a reduced displacement of 28% in Patient 3.

One of the concerns about the implantation of the PEARS is the formation of high stress regions at the unsupported portion of the aorta, a limitation shared with the aortic root replacement procedure. This study is the first attempt to address and quantify these concerns. From the stress analysis, peak stresses in the pre-PEARS models were located in the sinuses of Valsalva. The addition of the PEARS had an immediate effect on this peak stress which was not only increased significantly (in Patients 1 and 2), but also remained within the sinuses. Previous multilayer studies of stress distributions across the aorta have shown that the peak stress concentrates itself in the stiffest layers [27]. Upon integration of the PEARS into the aortic wall, stresses in the sinuses had reduced, while the peak stress was shifted to the aortic arch, particularly at the intersection between the supported and unsupported aorta, with corresponding increases of 183%, 156% and 89% for Patients 1, 2 and 3 respectively. This highly focal increase in the wall stress could lead to further weakening of the wall at these locations. Nevertheless, the peak stresses found in all the models presented here were well below the tensile strength for dilated ascending aortas, which was reported to be 1.18 ± 0.12 MPa in the circumferential direction and 1.21 ± 0.09 MPa in the longitudinal direction [28]. Another possible consequence of the focal increase in

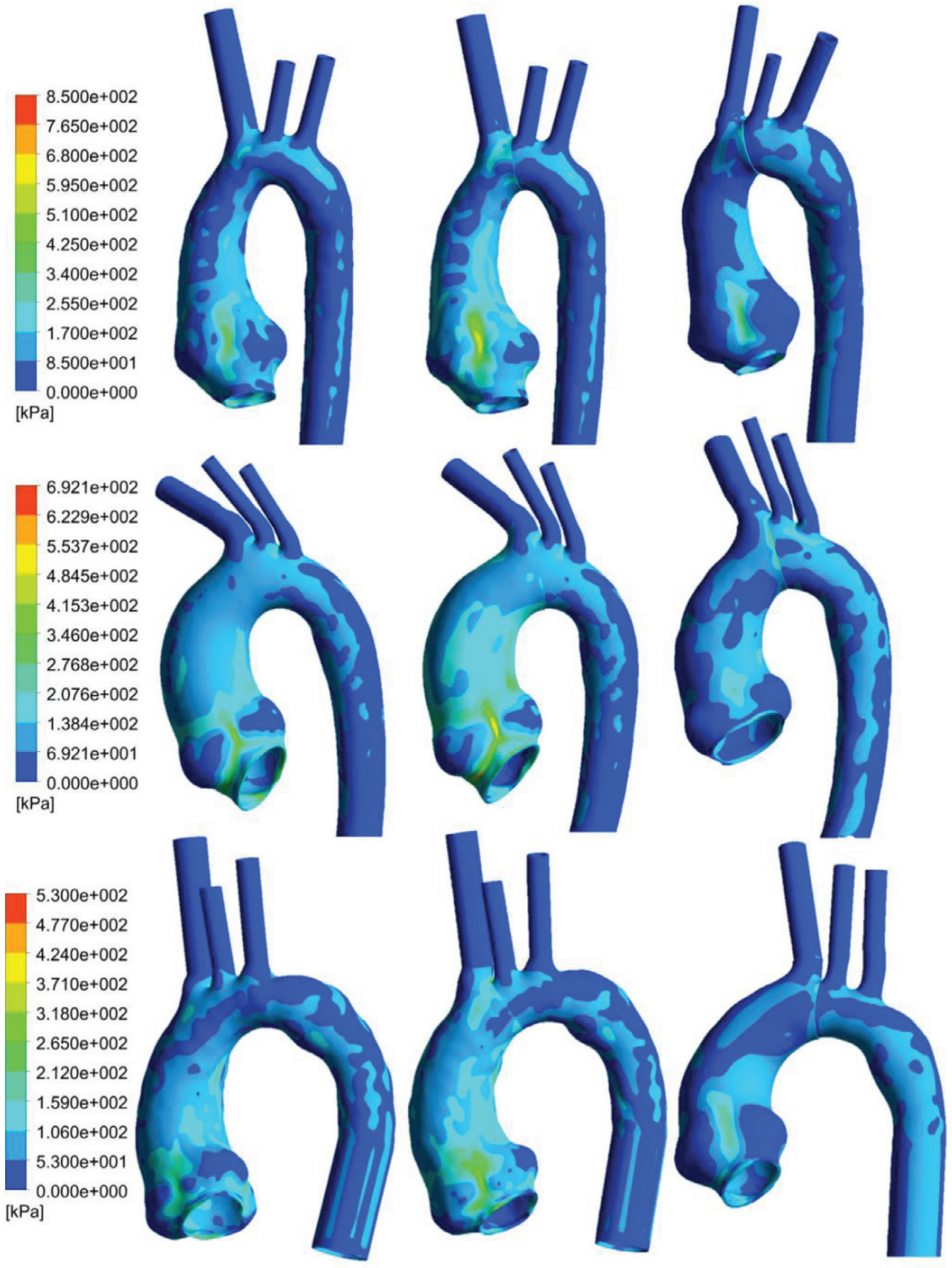

Fig. 6. Stress distribution in Patients 1, 2 and 3 (from L-R: pre-PEARS, post-PEARS bilayer and post-PEARS single-layer).

stress at these regions is aortic remodelling [29]. The ability of the aorta to remodel itself under applied loads and stresses can result in variation in wall thickness along the aorta.

5. Limitations

There are several limitations associated with the models developed in this study. One of the most important simplifications in these analyses is the constitutive equation, which describes the structural behaviour of the aortic wall. The aorta is multi-layered, heterogeneous and anisotropic, and upon loading, it undergoes large deformation and stiffening under increased pressures. Mechanical testing of samples of excised aortic tissue, healthy and diseased, has enabled the development of various types of non-linear constitutive relations [30,31]. However, data on the mechanical properties of the Marfan aorta are limited. The incremental elastic moduli and distensibility have been measured *in vivo* and the Marfan aorta is found to be significantly stiffer than normal aorta [17,19]. Alternatively,

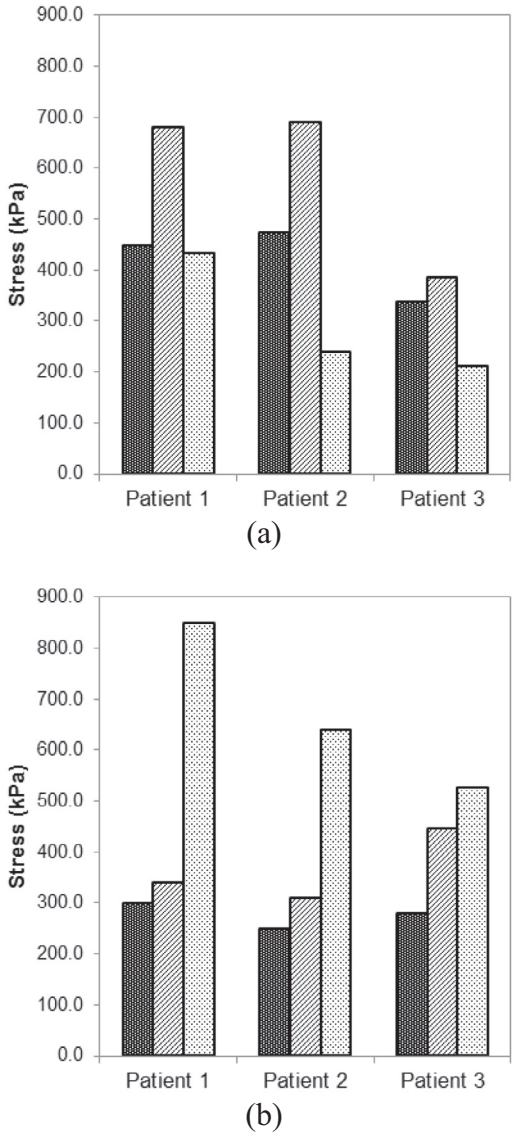

Fig. 7. Maximum von Mises stress in the sinus of Valsalva (a) and aortic arch (b) obtained from the ▦ Pre-PEARS, ▨ Post-PEARS (bilayer) and ⁘ Post-PEARS (single-layer) models for Patients 1, 2 and 3.

studies by Okamoto et al. [22,23] and Auricchio et al. [15] have focused on dilated ascending aorta, using hyperelastic constitutive formulations to describe the properties of the aorta. However, although these data are available for dilated aortas, no information is available on the supported (sleeved) Marfan aorta. Therefore, for comparative reasons, the linear-elastic constitutive formulation was employed in this study, pending acquisition of more realistic data supported by experimental studies.

The implications of using a simplified constitutive model were investigated by comparing results obtained with the linear elastic model and a hyperelastic two-parameter Mooney–Rivlin model. The pre-PEARS geometry of Patient 1 was used in this analysis. Qualitatively, the stress and strain distributions were similar. The patterns revealed that the high stress and strain regions were located at the sinus of Valsalva and the aortic arch in both models. Quantitatively, there were differences between the two models: the maximum stress in the sinus was 7% higher with the hyperelastic model while the strain at the same location was 62% lower. Despite these quantitative differences, the pre- and post-PEARS models in the current study were developed using identical conditions, with differences in only the geometry (patient-specific) and material properties. Therefore, comparison between the models is still valid, which provides an estimate of the relative differences that could be expected *in vivo* as a result of the insertion of the PEARS.

Also, the aortic wall thickness was assumed constant throughout the aorta due to insufficient spatial resolution of the MRI protocol adopted for *in vivo* scans, which were acquired in a clinical context. This is a common assumption adopted by several authors and its influence on predicted wall stress has been addressed by others [32,33]. The boundary between the aortic wall and lumen was crudely visible in some MR images, from which rough estimates of the thickness were obtained. However, lack of contrast between the aortic wall and lumen in most images made measurement of the wall thickness along the length of the aorta impossible.

In this study, the applied load corresponded to the patient's pulse pressure rather than the actual pressure, where increases in stress were taken as incremental changes from the diastolic state. In reality, a zero-stress state does not exist *in vivo*, however, it was found that the magnitude of residual stresses were negligible (up to 3 kPa [34]) in comparison with the aortic root stresses observed at the peak pressure. However, it must be acknowledged that residual stresses and strains act in homogenising the stress field in the arterial wall and allows greater compliance [35].

Additional limitations to the current model arise from the boundary conditions employed, one of which is the application of a uniform static load which corresponds to the patients' pulse

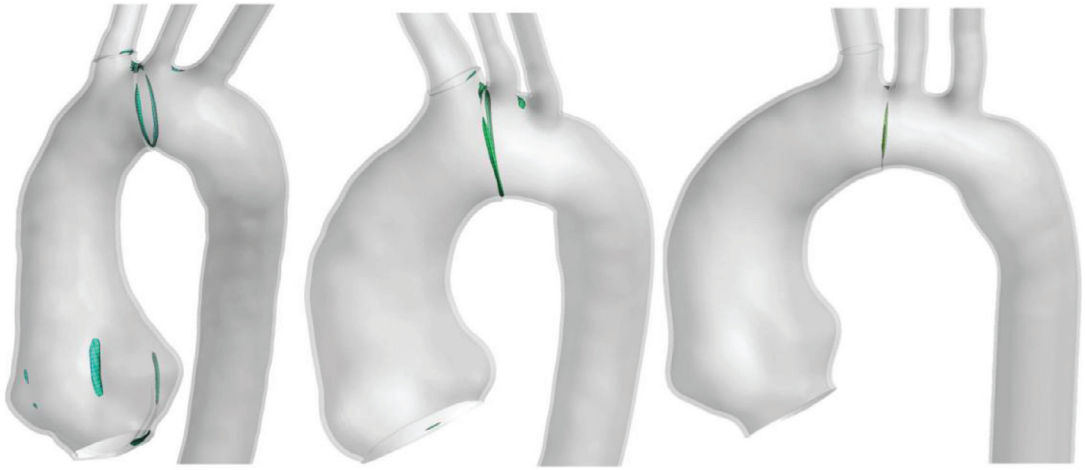

Fig. 8. Regions of stress greater than 290 kPa in the post-PEARS (single-layer) models for Patients 1, 2 and 3.

pressure. However, in reality, this pressure will vary both spatially and temporally. Borghi et al. [33] found very small differences (0.1–3.4%) in the predicted peak wall stress resulting from fluid-structure interaction simulations (which employ a time-dependent pressure waveform) and static structural analysis. Another boundary condition imposed on the aortic model was the constraining of the aortic root to zero-displacement to simulate the tethering to the rest of the aorta. Although this is a common assumption adopted by other researchers [15,35,36], in reality the ventricular contraction accompanying every heartbeat results in the motion of the aortic root, which may in turn have a direct influence on the deformation of the ascending aorta and the stress exerted on the aortic wall [37]. Future improvements to the model will involve extracting patient-specific aortic root motion from MR images and applying it as a more realistic boundary condition.

6. Conclusion

This study provides a preliminary biomechanical analysis of the Marfans' aorta of three patients having undergone implantation of the PEARS using combined imaging and computational modelling. Finite element simulations were performed using patient-specific geometries and pressures (pre- and post-PEARS). The stress and displacement distributions were investigated to evaluate the effects of the external support on the biomechanics of the aorta. The results showed that while the support reduced the displacement and stress distributions in the aortic root, particularly in the sinuses of Valsalva, stresses at the intersection between the supported and unsupported aorta were increased. Further studies are required to assess the statistical significance and clinical relevance of these findings.

Conflict of interest

None declared.

Ethical approval

Ethical Approval was given by the local Research Ethics Committee at the Royal Brompton & Harefield NHS Foundation Trust.

Acknowledgments

The author is grateful to Mr Tal Golesworthy (Extent Ltd, Tewkesbury, UK) for providing material data of PEARS and CAD models used to produce the PEARS. Shelly Singh is supported by a PhD scholarship from the Government of the Republic of Trinidad and Tobago.

References

[1] Judge DP, Dietz HC. Marfan's syndrome. The Lancet 2005;366:1965–76.
[2] Silverman DI, Gray J, Roman MJ, Bridges A, Burton K, Boxer M, et al. Family history of severe cardiovascular disease in Marfan syndrome is associated with increased aortic diameter and decreased survival. J Am Coll Cardiol 1995;26:1062–7.
[3] Ramirez F, Dietz HC. Marfan syndrome: from molecular pathogenesis to clinical treatment. Curr Opin Genet Dev 2007;17:252–8.
[4] Keane MG, Pyeritz RE. Medical management of Marfan syndrome. Circulation 2008;117:2802–13.
[5] Dormand H, Mohiaddin RH. Cardiovascular magnetic resonance in Marfan syndrome. J Cardiovasc Magn Reson: official journal of the Society for Cardiovascular Magnetic Resonance 2013;15:33.
[6] Hiratzka LF, Bakris GL, Beckman JA, Bersin RM, Carr VF, Casey Jr DE, et al. ACCF/AHA/AATS/ACR/ASA/SCA/SCAI/SIR/STS/SVM guidelines for the diagnosis and management of patients with thoracic aortic disease: a report of the American College of Cardiology Foundation/American Heart Association Task Force on Practice Guidelines, American Association for Thoracic Surgery, American College of Radiology, American Stroke Association, Society of Cardiovascular Anesthesiologists, Society for Cardiovascular Angiography and Interventions, Society of Interventional Radiology, Society of Thoracic Surgeons, and Society for Vascular Medicine. Circulation 2010;121:e266–369.
[7] Bentall H, De Bono A. A technique for complete replacement of the ascending aorta. Thorax 1968;23:338–9.
[8] David TE, Feindel CM, Bos J. Repair of the aortic valve in patients with aortic insufficiency and aortic root aneurysm. J Thorac Cardiovasc Surg 1995;109:345–52.
[9] Milewicz DM, Dietz HC, Miller DC. Treatment of aortic disease in patients with Marfan syndrome. Circulation 2005;111: e150-e7.
[10] Treasure T, Pepper J, Golesworthy T, Mohiaddin R, Anderson RH. External aortic root support: NICE guidance. Heart 2011;98:65–8.
[11] Pepper J, Golesworthy T, Utley M, Chan J, Ganeshalingam S, Lamperth M, et al. Manufacturing and placing a bespoke support for the Marfan aortic root: description of the method and technical results and status at one year for the first ten patients. Interact Cardiovasc Thorac Surg 2010;10:360–5.
[12] Pepper J, John Chan K, Gavino J, Golesworthy T, Mohiaddin R, Treasure T. External aortic root support for Marfan syndrome: early clinical results in the first 20 recipients with a bespoke implant. J Royal Soc Med 2010;103:370–5.
[13] Treasure T, Pepper JR. Aortic root surgery in Marfan syndrome. Heart 2011;97:951–2.
[14] Verbrugghe P, Verbeken E, Pepper J, Treasure T, Meyns B, Meuris B, et al. External aortic root support: a histological and mechanical study in sheep. Interact Cardiovasc Thorac Surg 2013;17:334–9.
[15] Auricchio F, Conti M, Demertzis S, Morganti S. Finite element analysis of aortic root dilation: a new procedure to reproduce pathology based on experimental data. Comput Method Biomec 2011;14:875–82.
[16] Grande-Allen KJ, Cochran RP, Reinhall PG, Kunzelman KS. Mechanisms of aortic valve incompetence: finite-element modeling of Marfan syndrome. J Thorac Cardiovasc Surg 2001;122:946–54.
[17] Vitarelli A. Aortic wall mechanics in the Marfan syndrome assessed by transesophageal tissue Doppler echocardiography. Am J Cardiol 2006;97:571–7.
[18] Baumgartner D, Baumgartner C, Matyas G, Steinmann B, Loffler-Ragg J, Schermer E, et al. Diagnostic power of aortic elastic properties in young patients with Marfan syndrome. J Thorac Cardiovasc Surg 2005;129:730–9.
[19] Sonesson B, Hansen F, Lanne T. Abnormal mechanical-properties of the aorta in Marfans-syndrome. Eur J Vasc Surg 1994;8:595–601.
[20] Hirata K, Triposkiadis F, Sparks E, Bowen J, Wooley CF, Boudoulas H. The Marfan syndrome: abnormal aortic elastic properties. J Am Coll Cardiol 1991;18:57–63.
[21] Jeremy RW, Huang H, Hwa J, McCarron H, Hughes CF, Richards JG. Relation between age, arterial distensibility, and aortic dilatation in the Marfan syndrome. Am J Cardiol 1994;74:369–73.
[22] Okamoto RJ, Wagenseil JE, DeLong WR, Peterson SJ, Kouchoukos NT, Sundt TM. Mechanical properties of dilated human ascending aorta. Ann Biomed Eng 2002;30:624–35.
[23] Okamoto RJ, Xu H, Kouchoukos NT, Moon MR, Sundt 3rd TM. The influence of mechanical properties on wall stress and distensibility of the dilated ascending aorta. J Thorac Cardiovasc Surg 2003;126:842–50.
[24] Nathan DP, Xu C, Plappert T, Desjardins B, Gorman 3rd JH, Bavaria JE, et al. Increased ascending aortic wall stress in patients with bicuspid aortic valves. Ann Thorac Surg 2011;92:1384–9.
[25] Weltert L, De Paulis R, Scaffa R, Maselli D, Bellisario A, D'Alessandro S. Recreation of a sinus like graft expansion in Bentall procedure reduces stress at the coronary button anastomoses: a finite element study. J Thorac Cardiovasc Surg 2009;137:1082–7.
[26] Vorp DA, Vande Geest JP. Biomechanical determinants of abdominal aortic aneurysm rupture. Arterioscler Thromb Vasc Biol 2005;25:1558–66.
[27] Gao F, Watanabe M, Matsuzawa T. Stress analysis in a layered aortic arch model under pulsatile blood flow. Biomed Eng Online 2006;5:25.
[28] Torii R, Xu XY, El-Hamamsy I, Mohiaddin R, Yacoub MH. Computational biomechanics of the aortic root. Aswan Heart Centre Science & Practice Series 2011;16:1–17.
[29] Rachev A. Remodelling of arteries in response to changes in their mechanical environment. CISM courses and lectures No 441 International Centre for Mechanical Sciences: biomechanics of soft tissue in cardiovascular systems. Holzapfel G, Ogden R, editors. New York: Springer-Verlag Wien; 2003.
[30] Holzapfel G, Gasser T, Ogden R. A new constitutive framework for arterial wall mechanics and a comparative study of material models. J Elast 2000;61:1–48.
[31] Gasser TC, Ogden RW, Holzapfel GA. Hyperelastic modelling of arterial layers with distributed collagen fibre orientations. J Royal Soc Interface 2006;3:15–35.
[32] Scotti CM, Shkolnik AD, Muluk SC, Finol EA. Fluid-structure interaction in abdominal aortic aneurysms: effects of asymmetry and wall thickness. Biomed Eng Online 2005;4:64.
[33] Borghi A, Wood NB, Mohiaddin RH, Xu XY. Fluid-solid interaction simulation of flow and stress pattern in thoracoabdominal aneurysms: a patient-specific study. J Fluid Struct 2008;24:270–80.
[34] Raghavan ML. Three-dimensional finite element analysis of residual stress in arteries. Ann Biomed Eng 2004;32:257–63.
[35] Conti CA, Votta E, Della Corte A, Del Viscovo L, Bancone C, Cotrufo M, et al. Dynamic finite element analysis of the aortic root from MRI-derived parameters. Med Eng Phys 2010;32:212–21.
[36] Grande-Allen KJ, Cochran RP, Reinhall PG, Kunzelman KS. Finite-element analysis of aortic valve-sparing: influence of graft shape and stiffness. IEEE Trans Bio-Med Eng 2001;48:647–59.
[37] Beller CJ, Labrosse MR, Thubrikar MJ, Robicsek F. Role of aortic root motion in the pathogenesis of aortic dissection. Circulation 2004;109:763–9.